Cardiovascular Research (2013) **97**, 262–270
doi:10.1093/cvr/cvs328

Myosin filament assembly onto myofibrils in live neonatal cardiomyocytes observed by TPEF-SHG microscopy

Honghai Liu[1†], Yonghong Shao[2†], Wan Qin[1†], Raymond B. Runyan[3], Meifeng Xu[4], Zhen Ma[1], Thomas K. Borg[5], Roger Markwald[5], and Bruce Z. Gao[1*]

[1]Department of Bioengineering and COMSET, Clemson University, Clemson, SC 29634, USA; [2]Institute of Optoelectronics, Shenzhen University, Shenzhen, Guangdong, PR China; [3]Department of Cellular and Molecular Medicine, University of Arizona, Tucson, AZ 85724, USA; [4]Department of Pathology and Laboratory Medicine, University of Cincinnati Medical Center, Cincinnati, OH 45267, USA; and [5]Department of Regenerative Medicine and Cell Biology, Medical University of South Carolina, Charleston, SC 29425, USA

Received 25 January 2012; revised 9 October 2012; accepted 26 October 2012; online publish-ahead-of-print 31 October 2012

Time for primary review: 55 days

Aims Understanding myofibrillogenesis is essential for elucidating heart muscle formation, development, and remodelling in response to physiological stimulation. Here, we report the dynamic assembly process of contractile myosin filaments onto myofibrils in a live cardiomyocyte culture during myofibrillogenesis.

Methods and results Utilizing a custom-built, two-photon excitation fluorescence and second harmonic generation imaging system equipped with an on-stage incubator, we observed new sarcomere additions in rat neonatal cardiomyocytes during 10 h of on-stage incubation. The new sarcomere additions occurred at the side of existing myofibrils, where we observed mature myofibrils acting as templates, or at the interstice of several separated myofibrils.

Conclusions During sarcomeric addition, myosin filaments are assembled onto the premyofibril laterally. This lateral addition, which proceeds stepwise along the axial direction, plays an important role in the accumulation of Z-bodies to form mature Z-disks and in the regulation of sarcomeric alignment during maturation.

Keywords Myofibrillogenesis • Sarcomere addition • Myosin filaments • Second harmonic generation • On-stage incubator

1. Introduction

Myofibrillogenesis is the process that assembles all protein components of a sarcomere and connects the sarcomeres to form myofibrils. Understanding myofibrillogenesis is essential to elucidate heart muscle formation, development, and remodelling in response to physiological stimulation. It is also critical to cardiac regulation in response to the mechanical load. Increase in diastolic strain causes cardiomyocytes to elongate by adding sarcomeres in series and continued systolic stress causes cardiomyocytes to thicken by adding sarcomeres in parallel.[1] Although the contractile components (e.g. actin and myosin filaments) and the structural components (e.g. the sarcomeric titin) are known to be synthesized separately before being assembled to form a mature sarcomere (*Figure 1*),[2–4] a model that describes the entire formation process of myofibrillogenesis has yet to be established due to lack of detailed information on the assembly process of each sarcomeric protein. Several models have been proposed to describe how sarcomeric components are assembled onto mature myofibrils[5–7]: (i) template model—stress fibre-like structures are thought to play the role of template or scaffold for myofibrillar assembly[5]; (ii) stitching model—sarcomeric components are thought to be assembled at the end of an existing myofibril by adding I-Z-I bodies and myosin filaments alternately[8–10]; and (iii) premyofibril model—the formation of myofibrils is thought to undergo three stages: premyofibrils, nascent myofibrils, and mature myofibrils. The three stages are distinguished by the substitution of muscle myosin II for non-muscle myosin IIB and the maturation of Z-disks from Z-bodies.[6,11,12] In the premyofibril stage, non-muscle myosin IIB is interdigitated with Z-bodies that contain alpha-actinin. In the nascent myofibril stage, muscle myosin II is substituted for non-muscle myosin IIB; this continues toward the mature myofibril stage, when all the non-muscle myosin IIB has been replaced by muscle myosin II.

† They are co-first authors.

* Corresponding author. Tel: +1 864 656 0185; fax: +1 864 656 4466, E-mail: zgao@clemson.edu

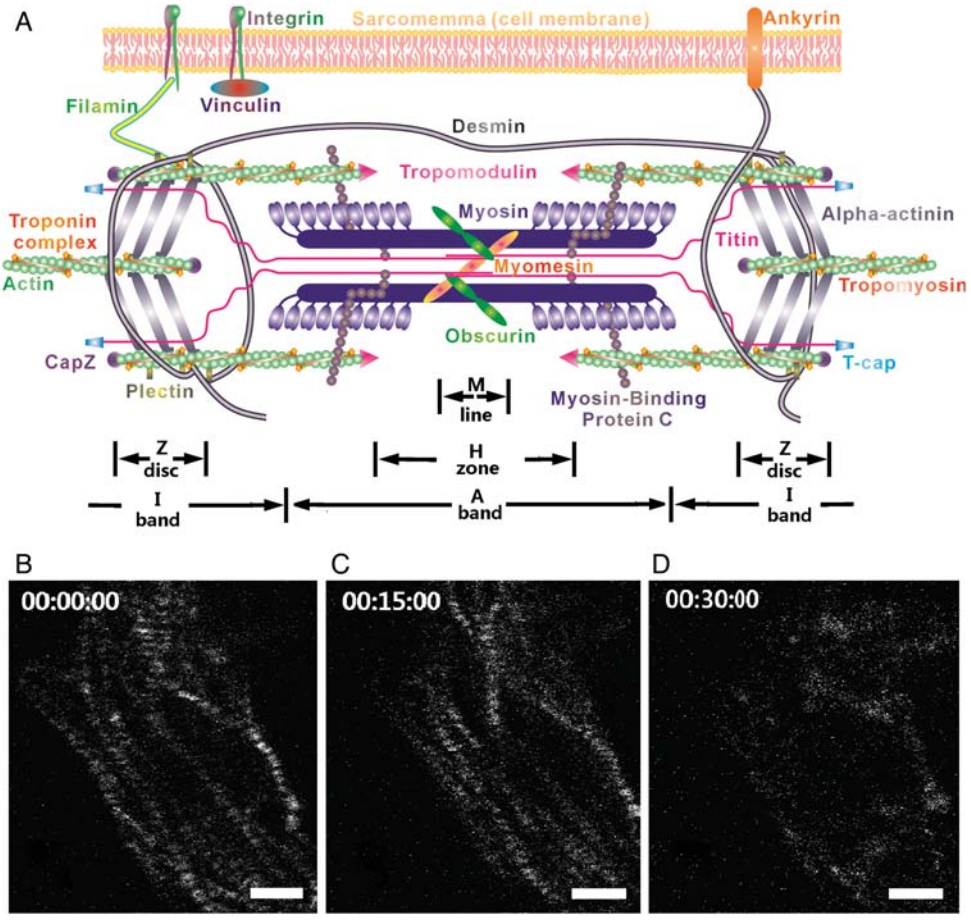

Figure 1 (*A*) Schematic of sarcomeric structure. (*B–D*) The change in the striated myofibril structure represented by the SHG pattern in three image acquisition trials. The time points are embedded in the hh:mm:ss format.

It has been demonstrated that sarcomeric components are not added simultaneously to the existing myofibrils; instead, different components are assembled successively on existing myofibrils, as described in the models above. The addition of myosin filaments is believed to be one of the final events in the process that leads to sarcomeric maturation.[3,13,14] It is unclear how myosin filaments are initially added onto myofibrils. Immunocytochemistry research based on myosin-filament staining has enhanced our understanding of myofibrillogenesis.[6] However, current fluorescence techniques can determine the position of the myosin proteins only from fixed cell samples and thus cannot be used to visualize the dynamic assembly process of myosin filaments.

Second harmonic generation (SHG) is intrinsic to certain specific structures; the SHG signal from cardiomyocytes arises from the coiled-rod structure of myosin filaments.[7] Therefore, the dynamic assembly of myosin filaments onto a myofibril may be studied without protein labelling.[8,9,15] Through the combination of two-photon excited fluorescence (TPEF) and SHG (TPEF–SHG), additional structural information can be obtained from a cardiomyocyte[10,11]; this microscopic technique is ideal for tracking how specific sarcomeric proteins are assembled onto myofibrils during myofibrillogenesis. Since myofibrillogenesis is a process that spans hours to days, we have developed a hybrid TPEF–SHG imaging system with an on-stage incubator that provides conditions that are close to the *in vitro* culture condition of isolated cardiomyocytes (e.g. 5% CO_2, 37°C, 95% humidity).[15]

Here, we report the dynamic process of myofibril formation in neonatal cardiomyocytes during 10 h of on-stage incubation. With the on-stage incubator and without the necessity of sarcomeric protein labelling, the system provides us with the ability to study the dynamic process of new sarcomere addition by directly monitoring the assembly of myosin filaments in living cardiomyocytes. The concepts explicated in the premyofibril model best describe our observations, and they will be adopted in our explanation of the experimental results and in Section 4.

2. Methods

2.1 TPEF–SHG imaging system with an on-stage incubator

The construction of the TPEF–SHG imaging system with an on-stage incubator is described in our previous publications.[12,15] The exciting laser beam was generated from a Ti:Sapphire laser (100 fs and 80 MHz, Tsunami 3960-X1BB pumped by a 10 W Millennia, Spectra-Physics) and was tuned to 810 nm. Our on-stage incubator was built based on the Okolab product (H301-TC1-HMTC, 2GF-MIXER, Okolab S.r.l., Ottaviano, NA, Italy), which is composed of an electronically heated

aluminum frame (slightly larger than a 96-well plate) with feedback control and two covers (top and bottom). We custom built the bottom cover for mounting our cell culture dish and the top cover for mounting our optical window. A mixture of 95% air and 5% CO_2 was pumped to go through the heater unit containing deionized (DI) water, and the humidified air mixture (~37°C, 95% humidity) was supplied to the chamber of the on-stage incubator. By design, the chamber was not completely sealed, and the 5% CO_2/95% humidity mixture was retained by adjusting the balance between the leakage and the supply through a feedback system. The 37°C temperature inside the culture dish was preserved by adjusting the balance between the heat loss and gain through a feedback system including a temperature sensor placed inside the media contained by the cell culture dish.

2.2 Image acquisition and cell viability assessment

During the imaging process, a cell was scanned continuously (a frame of 2D image) at a rate of 4 s per frame (spf), and the image data were saved in a virtual stack (~10–20 frames in 40–80 s) during each image acquisition trial. We performed one image acquisition trial every 15 min. Therefore, the selected cell was under continuous exposure in a period that was ~4–8% of the overall time of the experiment. To explore the risk of cell damage by the laser beam, we tested cell viability after each imaging process using a laser with a power that varied between 1 and 5 mW, a range used in a typical SHG imaging process. To achieve long-term observation, our experiment was designed to image a few individual cells selected from thousands of cells in each culture dish. Consequently, it was not feasible to use live/dead assays, such as LDH or CK-MB release, to study cell damage caused by the laser beam. Instead, we assessed cell viability based on morphologic changes. If after three image acquisition trials (~30 min) the cell lost its sarcomeric structure as reflected by the SHG signals shown in *Figure 1B–D*, the laser power would be considered harmful to cell viability. We found that for our imaging system, 2.8 mW was the optimum laser power to generate a strong SHG signal while maintaining cell viability. When fixed and stained cells were imaged, the average power of the incident fs laser beam was adjusted to ensure that the best image quality was obtained and the on-stage incubator was turned off. The virtual stack was processed and analyzed by ImageJ. (http://rsbweb.nih.gov/ij/)

Although a laser beam of 2.8 mW greatly improved cell viability, cell damage still occurred in our experiments. It has been reported that exposure of an fs laser at 810 nm may damage cells.[13,14,16] We observed myosin filament assembly in 20 growing cardiomyocytes in 6 experiments (i.e. 3–4 cells were scanned in each experiment). Among all the 20 cells, 1 cell showed no structural change in 10 h of on-stage incubation, 16 of them showed phenomena similar to that demonstrated in *Figure 1B–D* after several image acquisition trials (1–4 h): the structural changes were undistinguishable. The addition of new sarcomeres longitudinally along a myofibril or laterally perpendicular to the myofibril was observed in all three remaining cells.

2.3 Primary cardiomyocyte culture

Three-day-old Sprague–Dawley neonatal rats were euthanized by decapitation according to a procedure approved by the Clemson University Institutional Animal Care and Use Committee (Protocol number AUP2010-032); the procedure conforms with the Guide for the Care and Use of Laboratory Animals published by the US National Institutes of Health (NIH Publication, 8th Edition, 2011). The methods of euthanasia for neonatal animals are consistent with the recommendations of the Panel on Euthanasia of the American Veterinary Medical Association. The cardiomyocytes were collected as previously described.[15,17] Briefly, the heart was isolated and minced into 1 mm^3 pieces with scissors and first digested with trypsin solution (0.14 mg/mL without EDTA) overnight, then shaken at 75 rpm in a collagenase solution (1 mg/mL Collagenase II, GIBCO; 0.24 U/mL Neutral Protease, Worthington) for 1.5 h. The fibroblasts were removed by pre-incubating the cells in a 150-cm^2 flask with the culture medium [DMEM solution containing 20% foetal bovine serum (FBS)] for 2 h at 37°C. The purified cardiomyocyte (~90%) suspension was diluted to 100 K cells/ml and then seeded into 35-mm glass-bottom culture dishes coated with laminin (20 μg/mL). The cells were cultured in a conventional incubator (37°C and 5% CO_2). The culture medium (DMEM, 20% FBS) was changed after 24 h to remove dead cells and then was changed every 2 days.

2.4 TPEF–SHG and multichannel confocal imaging

After 1 day of culturing, one cardiomyocyte culture dish was placed into the on-stage incubator for live cell imaging using our TPEF–SHG imaging system. Simultaneously, cardiomyocytes in other dishes were fixed with absolute ethanol for 30 min at −20°C, then immersed in blocking solution (4% normal donkey serum, 0.02 mg/mL bovine serum albumin, 0.05% Triton X-100, dissolved in phosphate-buffered saline). Alpha-actinin was labelled by antibodies [(primary antibody: monoclonal alpha-actinin antibody from mouse (Sigma-Aldrich) and secondary antibodies: Alexa Fluor 488-conjugated donkey anti-mouse IgG (Invitrogen) or Rhodamine-conjugated goat anti-mouse IgG, (Millipore)]. F-actin was labelled with Alexa Fluor 488-conjugated phalloidin (Invitrogen). The stained cells were then mounted in the mounting solution containing DAPI (Invitrogen). A Nikon Eclipse Ti confocal microscope was applied for multichannel fluorescence image acquisition.

3. Results

According to the nature of the SHG images described in Section 1, here we accept the assumption that SHG signal patterns are images of the myosin filaments, and thus the striated SHG signal patterns indicate mature sarcomeric structures. To investigate the growth of myofibrils in live cardiomyocytes, we first observed, without cell staining, the SHG signal patterns that indicate the striated myofibrilar structure. A separation area located at the boundary of multiple mature myofibril segments was found to be filled with newly developed sarcomeres in a cardiomyocyte in the culture dish (*Figure 2*, arrow-a). The structural difference before and after the addition of sarcomeres was studied by analysing the grey value change in this area in Image J. Two additional mature sarcomeres were detected after being cultured on the stage for 8.5 h (*Figure 2E and F*, surrounded by rectangles). The mature sarcomeres were identified by peaks with doublets in the curves of grey value (characteristic of mature sarcomeres[18]). A propagation perturbation appeared at this separation area when a contraction wave was propagating from one segment to the other along the myofibrils (data not shown). However, the perturbation disappeared when the separation area was filled by mature sarcomeres. Therefore, the separation area (*Figure 2D*, arrow-a) appears to be the interstice where the divided myofibril sections unite into a single mature myofibril. The time-lapse image sequence (*Figure 2G*) demonstrates that during maturation of the sarcomeres at the separation area, the assembly of myosin filaments to the sarcomeres progressed laterally from one side of the sarcomeres to the other side.

At the beginning of the experiment, no apparent striated structure could be distinguished in the area indicated by arrow-b (*Figure 2A*). After on-stage incubation for 90 min, a striated structure gradually became distinguishable between the middle of the cell body and the

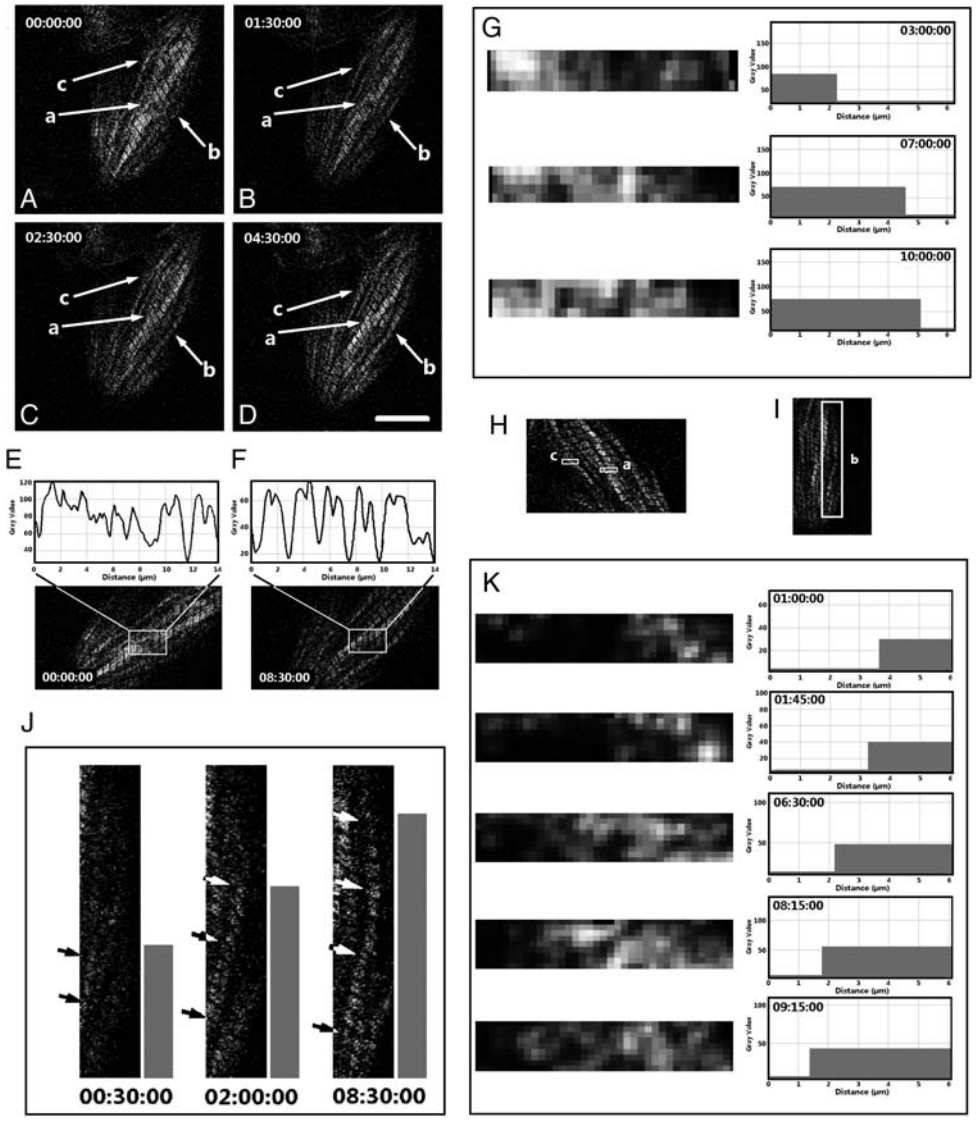

Figure 2 Sarcomeric addition in a live cell culture: the images were collected from the SHG channel, and the sample (cultured at Day 1) was a living cardiomyocyte isolated from a 3-day-old Sprague–Dawley neonatal rat. The dynamic process was detected at areas a–c (white arrows). (*A–D*) The myofibril structure at different time points. (*E* and *F*) The gray values of the SHG image indicated by arrow-a at 0 min and 8 h 30 min are plotted against the axial distance before and after new sarcomere addition. The images in (*E*) and (*F*) were obtained by rotating those in *A–D* at a specific angle to make the aligned Z-discs in the rectangles orient vertically; in this vertical direction, the pixel intensity was averaged and plotted against the axis of the myofibril that is oriented horizontally. (*G* and *K*) The time-lapse sequence of the gray values (against the lateral distance) in the areas indicated by inserted rectangles -a and -c in the SHG image shown in *H*. The corresponding horizontal bars were obtained by selecting a threshold gray value (e.g. 1/3 peak value) and binarizing the gray value images accordingly to demonstrate the lateral extension of sarcomeres from one side to the other. Similarly, the time-lapse images in *J* demonstrate the axial growth of a myofibril indicated by the inserted rectangle-b in *I* (the dynamic processes at areas b and c are displayed in the Supplementary material online, *Video S1* and *S2*, respectively; the time format in the videos is hh:mm:ss) (scale bar: 10 μm).

edge of the cell body (*Figure 2B–D*). The SHG signal is emitted from bundled myosin filaments,[7,19] so our time-lapse observation demonstrated the time sequence of myosin-bundle formation, accumulation, and addition to a myofibril. For example, it was observed that the myofibril length increased longitudinally with incubation time (*Figure 2A–D* arrow-b, and *I–J*; Supplementary material online, *Video S1*; the time format is hh:mm:ss). A similar phenomenon was observed at the area indicated by arrow-c (*Figure 2A–D*), where a new myofibril was added adjacent to the existing myofibrils during a 10-h time-lapse observation of SHG. Notably, as the myosin filaments were being assembled onto the new myofibrils (arrow-c), the direction of adding myosin filaments in a single sarcomere was from the adjacent mature myofibrils outwards (*Figure 2K* and the Supplementary material online, *Video S2*; the time format is hh:mm:ss).

Alpha-actinin has been recognized as one of the most important sarcomeric proteins present as the myofibrillogenesis begins.[20] The images displayed in *Figure 2* show only myosin filaments represented by the SHG signal patterns. To reveal how the myosin filaments are related to alpha-actinin during the formation and growth of myofibrils, we fixed the *in vitro* cultured neonatal cardiomyocytes

at Day 1 and immuofluorescently labelled the alpha-actinin. We then collected the fluorescence signal that represented the distribution of alpha-actinin from the TPEF channel of our imaging system and simultaneously collected the SHG signal that represented the distribution of myosin filaments from the SHG channel. Then alpha-actinin and myosin-filament images were reconstructed, assigned different colours, and combined.

Since our imaging system has only one TPEF channel, we employed a multichannel confocal microscope (Nikon Eclipse Ti microscope) to record the cell nucleus, alpha-actinin, and F-actin in one fluorescent image, and then inserted the myosin filament image that was recorded from the same cell with our TPEF–SHG imaging system (*Figure 3A–E*). To ensure the insertion would accurately maintain the relationship among alpha-actinin, F-actin, and myosin filaments during myofibrillogenesis, an image-matching operation was performed to linearly transform the TPEF–SHG image so that the alpha-actinin image obtained from the TPEF channel would perfectly overlap that obtained from the multichannel confocal microscope. Consequently, the correspondingly transformed myosin filament image (*Figure 3D*) from the SHG channel of the TPEF–SHG system would be under the same coordinate system as the other multichannel confocal images (*Figure 3A–C*).

Figures 3 and *4* are alpha-actinin/myosin filament (SHG signal patterns)-, or alpha-actinin/F-actin-combined images, which show that alpha-actinin and F-actin overlap to form small dots in the cell periphery (yellow arrows in *Figure 3E* and green arrows in *Figure 4E* and *F*). Similar small dots can be found in other images obtained from the TPEF–SHG imaging system (yellow arrowheads in *Figure 3G–I*; green arrows in *Figure 4B*). Alpha-actinin lines and myosin filaments from the TPEF–SHG imaging system formed an interdigitated pattern similar to that of striated mature myofibrils (*Figure 3F–K*). The detected myosin filaments were distributed mainly in the central area of the cells or in the middle section of the myofibrils at the boundary of the cells (*Figure 3F–H*). The alpha-actinin pattern (e.g. the long red strips in *Figure 4B*) extended laterally along the Z-disk direction, split into multiple strips while the myosin filaments gradually appeared, and became divided into segments along the myofibril direction to form the striated structure.

4. Discussion

In the time-lapse images from the SHG channel, the maturation of myofibrils from non-striated to striated pattern was recorded (*Figure 2J*, single arrows), but the involvement of other sarcomeric proteins in transition from non-striated to striated pattern cannot be determined in these images. To explore this transition in detail, we fluorescently stained alpha-actinin and F-actin in the cultured cardiomyocytes at Day 1 (*Figures 3* and *4*). Here, we assumed that the progressive assembly of sarcomeres to myofibrils that is observed using our time-lapse SHG would be recorded in a single static image obtained with the immunofluorescence imaging technique, and thus various myofibrillar growth patterns (e.g. those described by the premyofibril model) recorded by the time-lapse SHG would be reflected at various developing regions in the static image. Accordingly, the assembly process of the alpha-actinin and the myosin filament exhibited statically in *Figures 3* and *4* could be explained by the time-lapse images shown in *Figure 2*.

Based on the above consideration, the results are given the following descriptions: (i) in the confocal images, alpha-actinin and F-actin (e.g. indicated by yellow arrows in *Figure 3E* and green arrows in *Figure 4E* and *F*) overlap to form small dots, which we believe are Z-body structures described as premyofibrils in the premyofibril model. Similar small dots were found in the TPEF–SHG imaging system (e.g. indicated by yellow arrowheads in *Figure 3G–I*). Consequently, we assumed that the corresponding alpha-actinin images obtained through the TPEF channels, such as are indicated by the green arrows in *Figure 4B*, were indications of premyofibrils, although F-actin was not monitored simultaneously; (ii) for the same sample, striated mature myofibrils imaged by the confocal system coincided with the striated structures obtained by the TPEF–SHG imaging system (*Figure 3E*, red arrows), which is consistent with the accepted concept[16] that the striated structure obtained by the SHG imaging system is formed from myosin filaments; and (iii) the detected myosin filaments were distributed mainly in the central area of the growing cells or in the middle section of the myofibrils at the boundary of the growing cells (*Figure 3F–H*, and *J*).

In the present research, two types of myosin filament patterns, non-striated and striated, were observed in different areas of a growing cardiomyocyte (e.g. *Figure 4D*), which, as described above, corresponds to various assembly stages of myofibrils (e.g. *Figure 2J*). We consider that the premyofibril model best describes our observation because in our experiments, the three dynamic stages of myofibril formation (premyofibrils, nascent myofibrils, and mature myofibrils) predicted by the premyofibril model were observed in the assembling myofibrils: (i) alpha-actinin and F-actin staining dots were observed without simultaneous observation of myosin filaments at the early stage of myofibril formation (*Figure 3E*, yellow arrows); these observed structures have been recognized as premyofibrils.[3,12–14] (ii) Then, myosin filaments were observed, and the striated patterns of myosin filaments, alpha-actinin, and F-actin, which constitute nascent myofibrils at their late stage, began to form (*Figure 3K*). (iii) Finally, we observed perfectly aligned striated patterns of myosin filaments, alpha-actinin, and F-actin (*Figure 3E*, red arrows), which are characteristic of mature myofibrils. On the other hand, in addition to observing sarcomeric addition at the growing end of myofibrils,[15] we observed sarcomeric addition in the middle and at the side of developing myofibrils (*Figure 2*). Neither the stitching nor the template model can completely describe these additions.

Based on the above discussion of the stained alpha-actinin images, we can discuss the formation of Z-discs in terms of our results. Initially, the non-striated alpha-actinin-represented fibril extended laterally at the areas where myosin filaments have low density (*Figure 4B*, yellow arrowhead), which may correlate with the myosin filament's axial growing edge (*Figure 2J*). At this stage, no split of the fibrillar alpha-actinin pattern was found. Then, the extended alpha-actinin cluster became thinner along the myofibril's axial direction and elongated along the lateral direction when more myosin filaments were detected, which is demonstrated at the area where myosin filaments have higher density (*Figure 4B*, white arrow): This location may correlate with the myosin filament's axial growing front (*Figure 2J*). Finally, the extended alpha-actinin cluster became a thin line to form a mature Z-disc (*Figure 4B*, red arrowhead), which is shown at the area where myosin filaments have the highest density (*Figure 4B*, red arrow). This location may correlate with the myosin filament's axial growing section (*Figure 2J*).

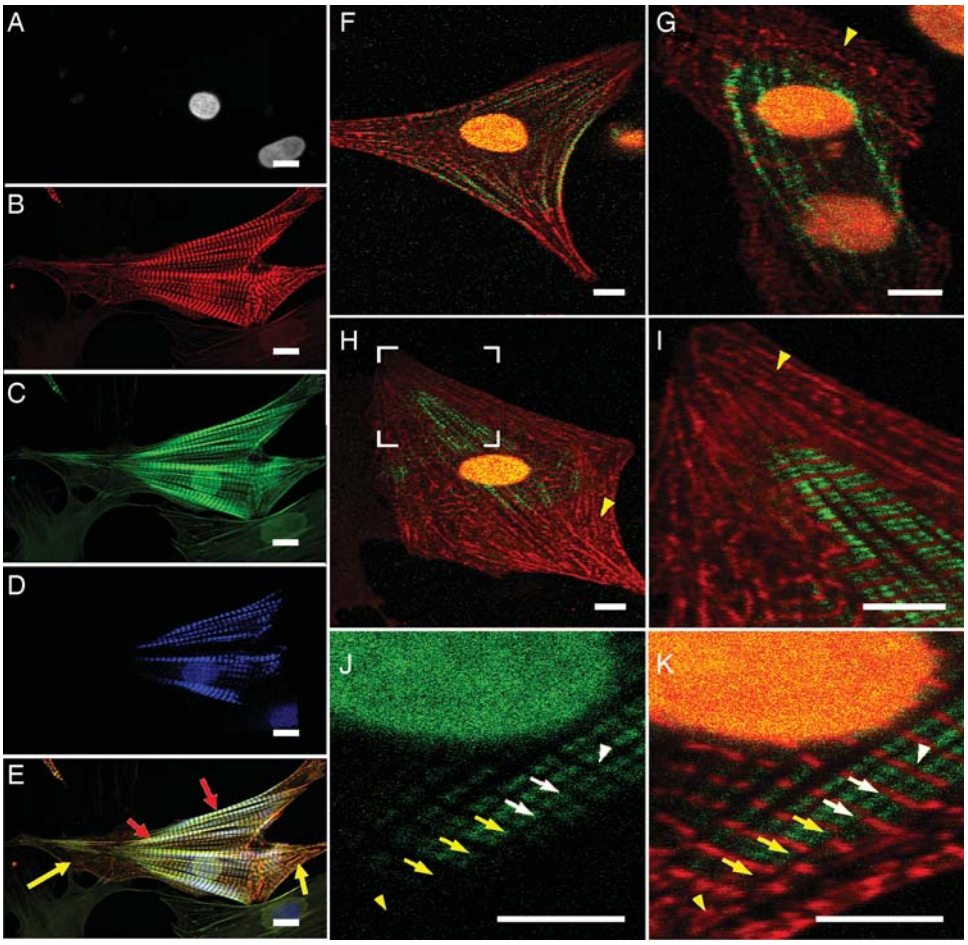

Figure 3 The myofibril structure of the cardiomyocytes isolated from 3-day-old Sprague–Dawley neonatal rats. (*A–C*) Confocal images (Nikon Ti microscope) of the nucleus, alpha-actinin, and F-actin fluorescently labelled by DAPI, alpha-actinin antibody, and phalloidin, respectively. (*D*) The myosin filament image of the same cellular sample as in *A–C* obtained from the SHG channel of our TPEF–SHG imaging system. (*E*) Combination of *A–D*. (*F–K*) TPEF–SHG images of alpha-actinin (red) and myosin filaments (green). The cells were fixed, and alpha-actinin was fluorescently labelled. The alpha-actinin pattern was acquired in the TPEF channel and the myosin filament pattern was acquired in the SHG channel. (*F*) A cell in which the striated alpha-actinin pattern (red) is colocalized with the SHG signal pattern (green) in the middle of the myofibrils at the cell edge. (*G*) A fused cell pair in which the striated alpha-actinin pattern (red) is co-localized with the SHG signal pattern (green) in the centre. (*H*) A cell in which the striated alpha-actinin pattern (red) is co-localized with the SHG signal pattern both in the cell centre and at the cell edge in the middle of the myofibrils. (*I*) Magnification of the area surrounded by the white bracket in *H*. The yellow arrowheads in *G–I* point to the short-term Z-bodies of premyofibrils. (*J* and *K*) Magnified SHG signal pattern (green) and alpha-actinin staining (red) of another cell; K is the SHG single pattern shown in J overlapped with the corresponding alpha-actinin pattern. The white arrowhead indicates the perfectly aligned Z-disks among adjacent mature myofibrils. The white arrows point to the Z-disks in adjacent myofibrils; these were connected to each other, but not perfectly aligned. The yellow arrows point to non-aligned striated alpha-actinin clusters. The yellow arrowhead points to an area with non-striated alpha-actinin clusters (premyofibrils) (scale bar: 10 μm)

Sparrow and Schöck reviewed a model proposed to extend the premyofibril model.[21] In this extended model, the bonding of Z-bodies to an integrin-dependent cell matrix adhesion was suggested as the starting point of myofibrillogenesis. Many techniques, such as the microcontact printing technique[22] and the collagen alignment technique,[23] have been applied to regulate the shape of cardiomyocytes and the orientation of myofibrils through controlling, outside the cell, the distribution of integrin-dependent cell matrix adhesions in the cell membrane. The success of these techniques supports the idea that the integrin-dependent cell matrix adhesion paves the way for myofibrillogenesis. Our data (*Figure 2*, arrows -b and -c) indicate that, in addition to the alignment of integrin-dependent cell matrix adhesions in the cell membrane, pre-existing myofibrils inside the cell can serve as a template for the alignment of the assembling myofibrils. The sarcomeric alignment of newly formed myofibrils with their neighboring mature myofibrils (*Figure 3K*) implies that pre-existing myofibrils may also play the role of a template and regulate the formation of new myofibrils. By comparing *Figure 3J* with *Figure 2J*, it can be seen that the patterns are similar in the areas denoted by the arrow and arrowhead in both figures, which implies that the arrow- and arrowhead-denoted myofibril in *Figure 3J* is at the assembly stage, similar to that represented in *Figure 2J* (02:00:00). Therefore, based on the point of view expressed in the first paragraph of this Section 4, we believe that the areas denoted

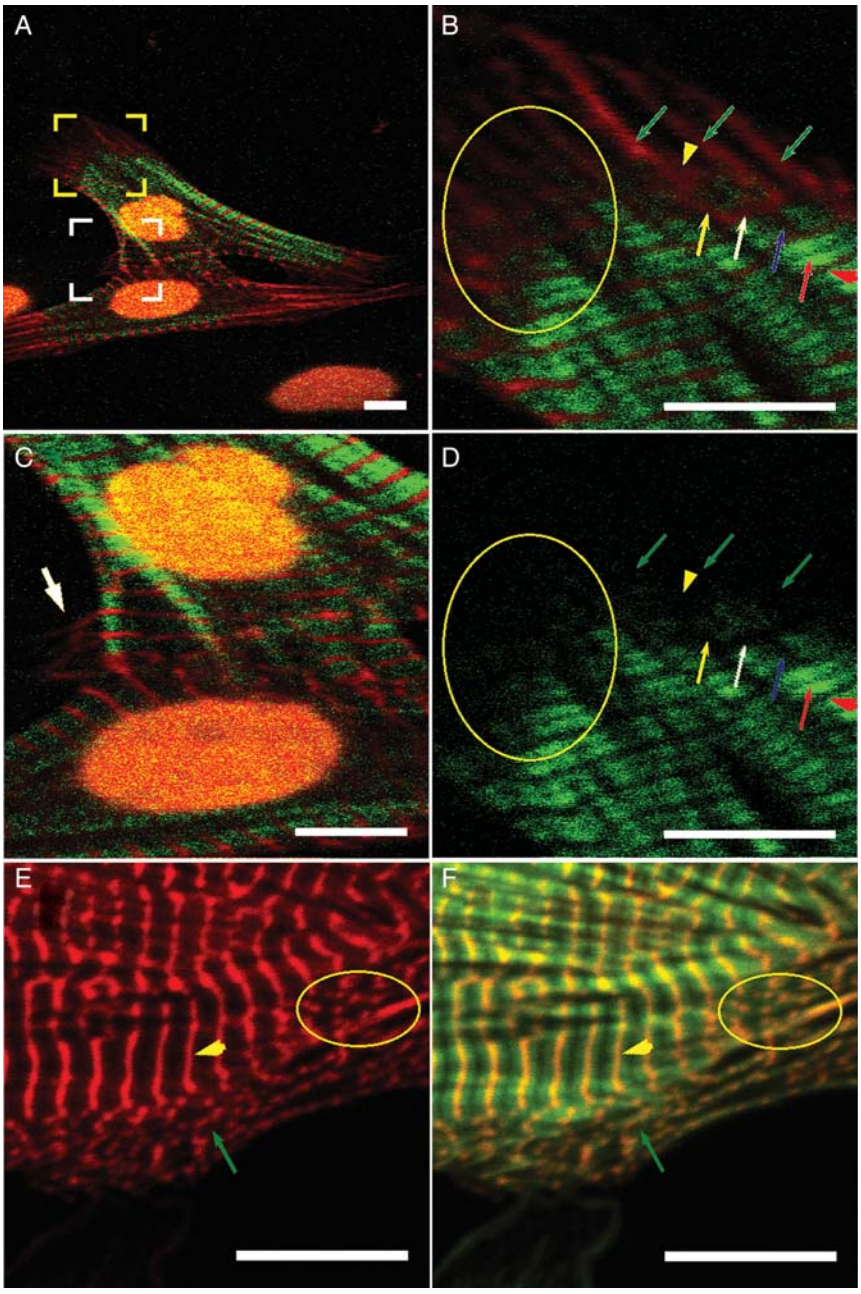

Figure 4 The myofibril structure in another group of cardiomyocytes isolated from 3-day-old Sprague–Dawley neonatal rats, cultured *in vitro* at Day 3. The cells were fixed and fluorescently labelled. (*A-C*) TPEF–SHG images—the alpha-actinin (red) pattern was acquired in the TPEF channel, and the green pattern was acquired in the SHG channel. (*A*) The myofibril structure of two connected cardiomyocytes. (*B*) Magnification of the area surrounded by the yellow brackets in (*A*). Green arrows: premyofibril—only the alpha-actinin pattern appeared along the direction of the myofibrils, where no SHG signal was detected; yellow arrowhead: lateral extension of the alpha-actinin pattern at the site where the Z-disk will appear in the future; yellow arrow: nascent myofibril—one alpha-actinin branch extended laterally and was connected with two alpha-actinin branches where the SHG signal pattern appeared; white arrow: the laterally extended alpha-actinin pattern became thinner when the SHG signal pattern appeared on both sides along the myofibril direction; blue arrow: the laterally extended alpha-actinin pattern became thinner when the SHG signal pattern on both sides of it was intensified to replace the alpha-actinin at the future A-band area; red arrow: mature sarcomere—the split alpha-actinin pattern had completely disappeared at the A-band area; red arrowhead: smooth laterally extended alpha-actinin pattern at the Z-disk area. Similar splits of the alpha-actinin pattern were found at most areas where the transition from non-striation to striation occurred (e.g. the area enclosed by the yellow ellipse in (*B*)). (*C*) Magnification of the area surrounded by the white brackets in (*A*). The white arrow indicates where the alpha-actinin pattern in Z-disks extended laterally from the striated myofibril structure at the area where the two cardiomyocytes connected. (*D*) The green-channel image of *B* showing only the SHG signal pattern. (*E* and *F*) Confocal images of double-stained alpha-actinin (red) and F-actin (green) from another cell sample acquired with a Nikon Eclipse Ti microscope. *E* is the red-channel image and *F* is an overlapped image from the red and green channels. The yellow arrowheads point to the striated (mature) myofibrils and the green arrows point to the dotted pre-myofibrils. An area of nascent myofibrils (transition from non-striation to striation) is circled by the yellow ellipse (scale bar: 10 μm).

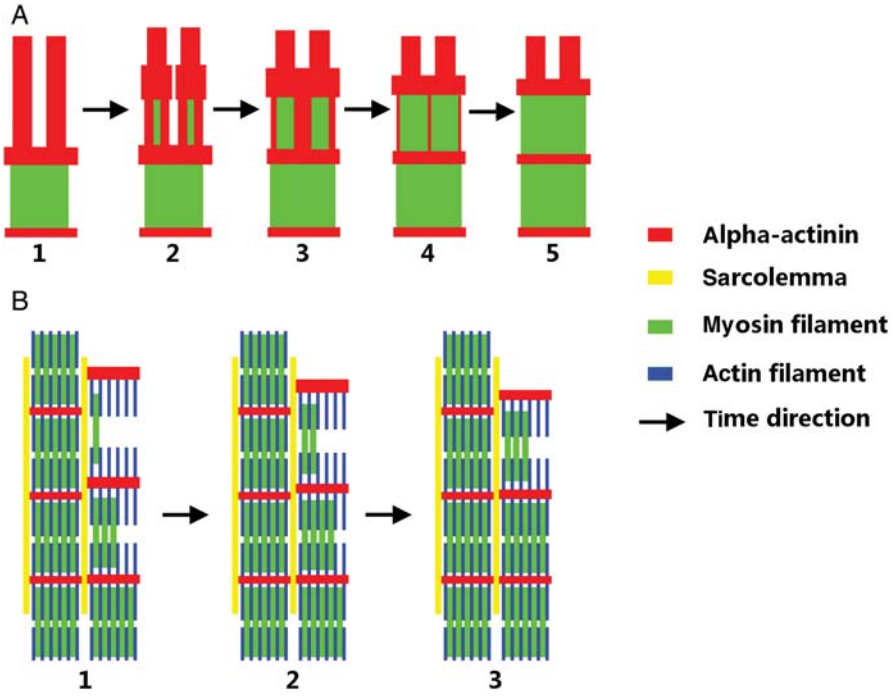

Figure 5 Proposed model of the lateral assembly of myosin filaments onto myofibrils of mature sarcomeres. (*A*) The assembly of myosin filaments splits the premyofibrils, rearranges the alpha-actinin to the Z-disk area, and removes alpha-actinins from the A-band area. (*B*) The alignment of the growing myofibril is affected by the adjacent mature myofibril. The growing myofibril aligns along the mature myofibril, and the Z-disks of a growing myofibril connect and merge with the adjacent Z-disks in the neighboring mature myofibril. The Z-disks become thinner during the maturation of the myofibril as myosin filaments assemble to the myofibril.

by white arrowhead, white/yellow arrows, and yellow arrowhead in *Figure 3J* and *K*, respectively, represent mature, nascent, and pre-myofibrils. Consequently, the alignment of the Z-discs of the growing myofibril from one end to the other with its neighboring mature myofibril suggests the templating process of the formation of new myofibrils.

Based on these results, we propose a model to describe the addition of myosin filaments to existing myofibrils (*Figure 5*). Initially, the aligned premyofibril (*Figure 5A*, red) is split by the lateral assembly of myosin filaments (*Figure 5*, A1–A4); this process removes the alpha-actinin at the A-band area, and condenses the alpha-actinin at the Z-disc area, until the sarcomere matures (*Figure 5*, A5). This lateral addition of myosin filaments proceeds stepwise along the axial direction to mature myofibrils (*Figure 5*, B1∼B3), and the mature myofibrils then regulate the alignment of the growing myofibrils, probably through the connection of sarcolemma related proteins (*Figure 5B*, yellow) such as desmin at the Z-disk area.

In terms of the data presented here and our previously published data,[15] we conclude that new sarcomere addition can occur at both the ends and the sides of existing myofibrils and at the interstice of several separated, existing myofibrils. During the addition of sarcomeres, myosin filaments are assembled onto the myofibril laterally. This lateral addition proceeds stepwise along the axial direction and plays an important role in the accumulation of Z-bodies to form mature Z-discs and in correlating the growing myofibrils with the neighboring mature myofibrils. Our results provide insight into the mechanism of assembly of myosin filaments during the addition of new sarcomeres onto the myofibrils. This could promote understanding of the mechanism of cardiac hypertrophy, especially pathological hypertrophy and the development of therapeutic techniques.

Supplementary material

Supplementary material is available at *Cardiovascular Research* online.

Acknowledgements

We would like to thank Dr Jeffrey W. Holmes at University of Virginia for invaluable discussions.

Conflict of interest: none declared.

Funding

This work was supported by National Institute of Health (P20RR021949 and 1k25hl088262-01); National Science Foundation (MRI CBET-0923311 and SC EPSCoR RII EPS-0903795 through SC GEAR program); The National Natural Science Foundation of China (31171372); and the Key Laboratory of Optoelectronic Devices and Systems of Ministry of Education and Guangdong Province (Shenzen University).

References

1. Russell B, Curtis MW, Koshman YE, Samarel AM. Mechanical stress-induced sarcomere assembly for cardiac muscle growth in length and width. *J Mol Cell Cardiol* 2010;**48**:817–823.
2. Carroll S, Lu SJ, Herrera AH, Horowits R. N-RAP scaffolds I-Z-I assembly during myofibrillogenesis in cultured chick cardiomyocytes. *J Cell Sci* 2004;**117**:105–114.

3. Ehler E, Rothen BM, Hammerle SP, Komiyama M, Perriard JC. Myofibrillogenesis in the developing chicken heart: assembly of Z-disk, M-line and the thick filaments. *J Cell Sci* 1999;**112**:1529–1539.
4. Clark KA, McElhinny AS, Beckerle MC, Gregorio CC. Striated muscle cytoarchitecture: an intricate web of form and function. *Ann Rev Cell Dev Biol* 2002;**18**:637–706.
5. Dlugosz AA, Antin PB, Nachmias VT, Holtzer H. The relationship between stress fiber-like structures and nascent myofibrils in cultured cardiac myocytes. *J Cell Biol* 1984;**99**:2268–2278.
6. Du AP, Sanger JM, Linask KK, Sanger JW. Myofibrillogenesis in the first cardiomyocytes formed from isolated quail precardiac mesoderm. *Dev Biol* 2003;**257**:382–394.
7. Plotnikov SV, Millard AC, Campagnola PJ, Mohler WA. Characterization of the myosin-based source for second-harmonic generation from muscle sarcomeres. *Biophys J* 2006;**90**:693–703.
8. Nucciotti V, Stringari C, Sacconi L, Vanzi F, Fusi L, Linari M *et al*. Probing myosin structural conformation in vivo by second-harmonic generation microscopy. *P Natl Acad Sci USA* 2010;**107**:7763–7768.
9. Prent N, Green C, Greenhalgh C, Cisek R, Major A, Stewart B *et al*. Intermyofilament dynamics of myocytes revealed by second harmonic generation microscopy. *J Biomed Opt* 2008;**13**:041318.
10. Barzda V, Greenhalgh C, der Au JA, Elmore S, van Beek JHG, Squier J. Visualization of mitochondria in cardiomyocytes by simultaneous harmonic generation and fluorescence microscopy. *Opt Express* 2005;**13**:8263–8276.
11. Wallace SJ, Morrison JL, Botting KJ, Kee TW. Second-harmonic generation and two-photon-excited autofluorescence microscopy of cardiomyocytes: quantification of cell volume and myosin filaments. *J Biomed Opt* 2008;**13**:640181–640185.
12. Shao Y, Liu H, Ye T, Borg T, Qu J, Peng X *et al*. 3D myofibril imaging in live cardiomyocytes via hybrid SHG-TPEF microscopy. *Proceedings of SPIE* 2011;7903: 79030F79031–79036.
13. Barzda V, Greenhalgh C, Aus der Au J, Elmore S, van Beek J, Squier J. Visualization of mitochondria in cardiomyocytes by simultaneous harmonic generation and fluorescence microscopy. *Opt Express* 2005;**13**:8263–8276.
14. Huang S, Heikal AA, Webb WW. Two-photon fluorescence spectroscopy and microscopy of NAD(P)H and flavoprotein. *Biophys J* 2002;**82**:2811–2825.
15. Liu H, Qin W, Shao Y, Ma Z, Ye T, Borg TK *et al*. Myofibrillogenesis in live neonatal cardiomyocytes observed with hybrid two-photon excitation fluorescence-second harmonic generation microscopy. *J Biomed Opt 16(12)*, 2011;**16**:1260121–1260124.
16. Major A, Cisek R, Greenhalgh C, Prent N, Stewart B, Barzda V. Ytterbium-ion femtosecond laser reduces damage during biomedical imaging. *SPIE Newsroom*. Advance Access Published December 13, 2006, doi:10.1117/2.1200611.0497.
17. Ma Z, Pirlo RK, Wan Q, Yun JX, Yuan XC, Xiang P *et al*. Laser-guidance-based cell deposition microscope for heterotypic single-cell micropatterning. *Biofabrication* 2011;**3**:034107.
18. Recher G, Rouede D, Richard P, Simon A, Bellanger JJ, Tiaho F. Three distinct sarcomeric patterns of skeletal muscle revealed by SHG and TPEF microscopy. *Opt Express* 2009;**17**:19763–19777.
19. Campagnola PJ, Millard AC, Terasaki M, Hoppe PE, Malone CJ, Mohler WA. Three-dimensional high-resolution second-harmonic generation imaging of endogenous structural proteins in biological tissues. *Biophys J* 2002;**82**:493–508.
20. Sanger JW, Kang S, Siebrands CC, Freeman N, Du A, Wang J *et al*. How to build a myofibril. *J Muscle Res Cell Motil* 2005;**26**:343–354.
21. Sparrow JC, Schöck F. The initial steps of myofibril assembly: integrins pave the way. *Nat Rev Mol Cell Bio* 2009;**10**:293–298.
22. Bray MA, Sheehy SP, Parker KK. Sarcomere alignment is regulated by myocyte shape. *Cell Motil Cytoskel* 2008;**65**:641–651.
23. Walsh KB, Parks GE. Changes in cardiac myocyte morphology alter the properties of voltage-gated ion channels. *Cardiovas Res* 2002;**55**:64–75.